

# Spectrum of the QCD flux tube in 3d SU(2) lattice gauge theory

Bastian B. Brandt

*Institut für Kernphysik, Johannes Gutenberg-Universität Mainz,  
Johann Joachim Becher-Weg 45, D-55099 Mainz\**

Pushan Majumdar

*Dept. of Theoretical Physics, Indian Association for the Cultivation of Science, Jadavpur, Kolkata 700032.†*

Evidence from the lattice suggests that formation of a flux tube between a  $q\bar{q}$  pair in the QCD vacuum leads to quark confinement. For large separations between the quarks, it is conjectured that the flux tube has a behaviour similar to an oscillating bosonic string, supported by lattice data for the groundstate  $q\bar{q}$  potential. We measure the excited states of the flux tube in 3d SU(2) gauge theory with three different couplings inside the scaling region. We compare our results to predictions of effective string theories.

## I. INTRODUCTION

Simulations over the last few years have accumulated strong evidence that gluonic dynamics indeed leads to the formation of a flux tube between test quark and anti-quark ( $q\bar{q}$ ) in the vacuum of Yang-Mills theory, at least on the lattice [1]. This implies a linearly rising potential between quark and anti-quark in the QCD vacuum and thus leads to quark confinement again on the lattice at least. At large  $q\bar{q}$  separations, this flux tube is expected to behave like a string. Open bosonic string descriptions of the dynamics of this flux tube have been attempted for a long time [2]. Using the Nambu-Goto (NG) action, first *Alvarez* [3] (in the limit  $d \rightarrow \infty$ ) and later *Arvis* [4] obtained the energy states of the flux tube as

$$E_n(R) = \sigma R \sqrt{1 + \frac{2\pi}{\sigma R^2} \left( n - \frac{1}{24} (d-2) \right)} \quad (1)$$

where  $\sigma$  is the string tension,  $R$  the quark-antiquark separation and  $d$  the number of space-time dimensions. A closed string description was proposed by Polchinski and Strominger (PS) [5] where they suggested how effective string theory with vanishing conformal anomaly could be formulated in arbitrary dimensions. The spectrum of the string using the PS prescription has been computed in [6, 7, 8]. To order  $R^{-3}$  it has been found that the spectrum is universal (depends only on the number of space-time dimensions and the string tension), and to this order it coincides with the NG spectrum. For a calculation of the closed string spectrum on the lattice see [9]. Another interesting idea put forward by Lüscher and Weisz (LW) is that of open-closed string duality [10]. They showed that demanding this duality constrains the possible string spectra and in particular forbids  $1/R^2$  terms in the effective string action. In the LW formulation too, the spectrum is consistent with the NG spectrum. In

3-dimensions it is exactly the same and in 4-dimensions one undetermined parameter remains which can of course assume the NG value. The NG partition function itself respects open-closed duality. Predictions from these theories can be tested by comparing them to results coming from simulations of pure Yang-Mills theories.

In this article we will present a new scheme for measuring observables in simulations of pure Yang-Mills theories. Using this scheme we will accurately measure observables in 3-dimensional SU(2) lattice gauge theory and try to extract the excitation spectrum of the flux tube. For earlier studies of the QCD string spectra using different schemes in both 3 and 4 dimensions for several gauge theories, see [11] and the references therein.

## II. PRELIMINARIES

To probe the properties of the flux tube formed between test quark and anti-quark, the two observables in pure Yang-Mills theories are the Polyakov loop correlation function and spatio-temporal Wilson loops. While Polyakov loop correlation functions project very strongly onto the ground state, Wilson loops are much more sensitive to the excited states of the flux tube and in addition allows one to couple more strongly to a particular state while suppressing the others, by appropriate choice of the spatial parts of the loop. It is therefore the observable of choice if one wants to study the excitation spectrum of the flux tube.

### A. Extraction of the excited states

In three dimensions, the states of the oscillating string can be classified by charge-conjugation and parity properties ( $C, P$ ) [12, 13]. Choosing the spatial parts of the Wilson loops as shown in figure 1, the ( $C, P$ ) projectors

\*Electronic address: brandt@kph.uni-mainz.de

†Electronic address: tppm@iacs.res.in

are given by the superpositions

$$\begin{aligned}
\mathbb{S}^{++} &= \mathbb{S}_1 + \mathbb{S}_2 + \mathbb{S}_3 + \mathbb{S}_4 \\
\mathbb{S}^{+-} &= \mathbb{S}_1 + \mathbb{S}_2 - \mathbb{S}_3 - \mathbb{S}_4 \\
\mathbb{S}^{--} &= \mathbb{S}_1 - \mathbb{S}_2 - \mathbb{S}_3 + \mathbb{S}_4 \\
\mathbb{S}^{-+} &= -\mathbb{S}_1 + \mathbb{S}_2 - \mathbb{S}_3 + \mathbb{S}_4
\end{aligned} \tag{2}$$

where  $+/-$  stands for even or odd states under  $C$  and  $P$ . Although in each of the  $(C, P)$  channels, there are an infinite number of states, we are going to look only at the ground states and will label these channels as  $\{0, 1, 2, 3\}$

respectively. The Wilson loop projecting onto a channel  $n$  has the spectral representation

$$W_n(R, T) = \sum_{i=0}^{\infty} \beta_i(R) e^{-E_n^i(R) T}. \tag{3}$$

where  $E^i$  are the energies of the states in a given channel. Using Wilson loops with different temporal extents, one obtains the energies and energy differences at leading order as

$$-\frac{1}{T_b - T_a} \ln \left[ \frac{W_n(R, T_b)}{W_n(R, T_a)} \right] = E_n(R) + \frac{1}{T_b - T_a} \alpha_n(R) e^{-\delta_n(R) T_a} \left( 1 - e^{-\delta_n(R) (T_b - T_a)} \right) \tag{4}$$

$$-\frac{1}{T_b - T_a} \ln \left[ \frac{W_n(R, T_b) W_m(R, T_a)}{W_n(R, T_a) W_m(R, T_b)} \right] = \Delta E_{nm}(R) + \frac{1}{T_b - T_a} \alpha_n(R) e^{-\delta_n(R) T_a} \left( 1 - e^{-\delta_n(R) (T_b - T_a)} \right) \tag{5}$$

where  $T_a < T_b$ . In the following the values obtained from the LHS of eqns.(4) and (5) will be called naïve values  $\bar{E}_n(R)$  and  $\Delta \bar{E}_{nm}(R)$ , while  $E_n(R)$  and  $\Delta E_{nm}(R)$  which are obtained by fitting with  $\alpha_n$  and  $\delta_n$  as additional fit parameters will be called corrected values.

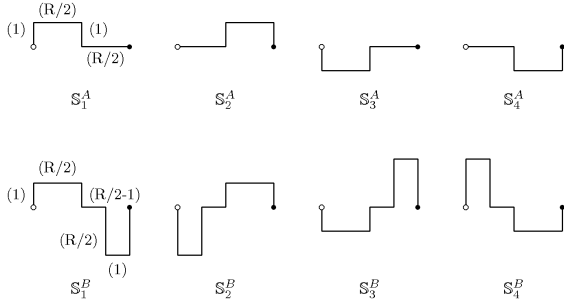


FIG. 1: **Top:** Basic set of operators used to construct  $(C, P)$  channels. **Bottom:** Set of operators with stronger coupling to the second excited state.

## B. Noise reduction techniques

String like behaviour of the flux tube is expected to occur at large  $q\bar{q}$  separations. The Wilson loops we measure must therefore extend to large enough  $R$  values. Also we see from equations (4) and (5) that to reduce the contaminations due to other states we must either go to large values of  $T$  or tune  $\alpha$  to small values by appropriate choice of the basis states. The latter method has been followed in [14] where asymmetric lattices with small temporal extents were used. The former method requires accurate measurements of expectation values of

large Wilson loops, made possible recently by the multilevel algorithm, proposed in [15]. This method has been used in [16, 17] to accurately measure the ground state properties of the flux tube. Here we will try to combine both methods by using a slight variant of the multilevel algorithm.

In the multilevel algorithm, intermediate averages are computed for the temporal links by updating certain sub-lattices with the sources on the spatial links of the boundaries of these sub-lattices. The boundaries are held fixed during the sub-lattice updates. We now put the sources on space-like surfaces in the middle of a sub-lattice of thickness  $2a$  where  $a$  is the lattice spacing. Two temporal links are attached to the two ends of the source which terminates on the space-like surfaces that are fixed during the sub-lattice updates (see fig.2). The advantage is that the sub-lattice updates reduces fluctuations of the sources as well as fluctuations of the temporal links. Moreover, in addition to using multihit on the temporal links, we can now use multihit on the spatial links as well. For further details see [12, 18] and references therein. Adopting the notation in [15], we now define the expectation value of the Wilson loop by

$$\langle W(T) \rangle = \langle \{ \mathbb{L}(0) \}_{\alpha\gamma} \{ \mathbb{T}(a) \cdots \mathbb{T}((T-1)a) \}_{\alpha\beta\gamma\delta} \{ \mathbb{L}(T)^* \}_{\beta\delta} \rangle, \tag{6}$$

where  $\mathbb{L}(t)$  is the operator of fig.2 and  $\{ \}$  indicates sub-lattice averaged quantities. The only difference from [15] is that now we have  $\{ \mathbb{L} \}$  instead of  $\mathbb{L}$ .

In most parts of the calculations, the operators  $\{ \mathbb{S}_i^A \}$  (figure 1 top; see also [13, 18]) are good enough for a reliable signal. However, for the second excited state beyond  $\beta = 7.5$  the error reduction was not sufficient and we had to use another set of operators  $\{ \mathbb{S}_i^B \}$ , (figure 1 bottom) with a stronger coupling to that particular excited state.

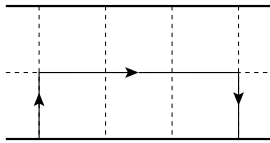


FIG. 2: The source of the Wilson loop in the modified algorithm. The product of the directed lines defines the source. The thick lines are held fixed during sub-lattice updates.

We will henceforth refer to the two sets as set  $A$  and set  $B$  respectively. To check the error reduction with the new set of operators we performed 460 measurements at  $\beta = 7.5$  with spatial extents  $R = 15 - 20$  using the simulation parameters shown in table I. The resulting relative errors of  $\bar{E}_2$  are also tabulated there. The values for the naïve energies using both sets are plotted in figure 3. For comparison we also plot  $E_2$ , which was calculated from  $\bar{E}_2^A$ , in the same region. We note that the value of set  $B$  is closer to the expectations shown by the black line and the corrected values. Set  $B$  however does not lead to improvement for the other states.

There are several parameters for the algorithm, that have to be tuned properly in order to achieve the maximal error reduction. For the temporal links we follow the same procedure as outlined in [13]. In addition we now have another parameter which is the number of updates ( $N_s$ ) for the sub-lattices containing the spatial operators. We found it beneficial for the excited states to have quite a large number of such sub-lattice updates. Since there are only two such sub-lattices for every loop this does not increase the cost of the simulation very much. Table II contains the resulting optimized run parameters and we refer to [12] for details of the optimization.

### C. Simulation parameters and lattice scales

Our simulations were done with three different couplings,  $\beta = 7.5, 10.0$  and  $12.5$  (chosen so as to lie in the scaling region) in three dimensional  $SU(2)$  lattice gauge theory, using usual heatbath sweeps [19], combined with three overrelaxation sweeps. The scale was set by the Sommer parameter  $r_0$  [20], which has been computed for these  $\beta$  values with high accuracy in [17]. For each beta value we calculated Wilson loops with four different temporal extents and used cubic lattices with extents large enough to ensure that finite size effects were significantly lower than our statistical errors. Our simulation parameters, together with the parameters for the multilevel al-

$T$	Lat	$t_s$	$N_s$	$N_t$	$R$	15	16	17	18	19	20
6	$36^3$	4	18000	1500	A	0.62	0.73	0.85	0.99	1.23	1.60
10	$40^3$	4	18000	2500	B	0.39	0.45	0.50	0.60	0.77	0.99

TABLE I: **Left:** Parameters of the testruns to compare the operators. **Right:** Relative error of  $\bar{E}_2$  in % for operator sets  $A$  and  $B$ .

gorithm are tabulated in table II.

### D. Error analysis and control of the fits

For estimating the error of all the energy values and differences, we used the usual binned jackknife method, with binsizes 44, 24, 40 and 40 for the lattices  $L^A$ ,  $L_A^B$ ,  $L_B^B$  and  $L^C$  respectively. We also checked that the errors did not vary by more than a few percent with bin size.

For the energy difference  $\Delta E_{20}$  at  $\beta = 10.0$  and  $12.5$  we used the results obtained from set  $B$  for  $E_2$  while the values for  $E_0$  were obtained from set  $A$ . Since these two values come from independent simulations, we added the individual errors in quadrature to obtain error estimates for  $\Delta E_{20}$ .

The remaining issue is the control of the fits (4) and (5), and this was done in two ways. For the energies  $E_n$ , we expect  $\alpha$  to be smaller than the ratio of the degeneracies [23] of the energy states considered and  $\delta$  should be of the order of the energy gap to the next level in the channel. Similar conclusions hold for the parameters of the energy differences [12, 13] as well. If the resulting fit parameters were far of from these expectations we did not trust the fits. As a second check, we plotted the expected corrections  $\Delta$ , obtained with averaged parameters  $\alpha_n$  and  $\delta_n$  against the differences  $\bar{\Delta} = E_n - \bar{E}_n$ , for all possible combinations of  $T_a$  and  $T_b$ . If for some of the values there was a big discrepancy to the expectation  $\Delta = \bar{\Delta}$  the fit was also regarded as unreliable (for more details see [12]).

## III. SIMULATION RESULTS

In this section we discuss the results of our simulations, that are tabulated in table IV. We compare to the full NG spectrum, eq.(1) and to leading order (LO) and next to leading order (NLO) models which are obtained by truncating the expansion of the square root of (1) in  $1/R^2$  at leading order and next to leading order respectively. The LW and PS type string theories give identical results to NLO order. The curves in the plots were drawn using the string tension at  $\beta = 12.5$ . All the results have been rescaled so that they are visible on a single plot.

### A. Energy states

We use the groundstate to determine the string tension and fix an additive constant  $V_0$ , appearing in the potential, by fitting to the form [4]:

$$V(R) = \sigma R \sqrt{1 - \frac{\pi}{12 \sigma R^2}} + V_0 \quad (7)$$

The results of the fits are shown in table III, where also the values from [17] are shown for comparison. We see that all results agree well within error bars. Also  $\sigma$  and  $V_0$  from both operator sets agree with each other.

Lat	$\beta$	$r_0$	$a$ [fm]	$R$	$\{S_i\}$	$T$	$T$ [fm]	$t_s$	size	$N_s$	$N_t$	#meas
$L^A$	7.5	6.2875(10)	0.07952(1)	7 – 20	A	6	0.477	4	38 <sup>3</sup>	36000	1500	4400
						10	0.795	4	40 <sup>3</sup>		3000	6468
						14	1.113	6	42 <sup>3</sup>		9000	11176
						18	1.431	4	54 <sup>3</sup>		18000	6512
$L_A^B$	10.0	8.6602(8)	0.05812(1)	9 – 27	A	8	0.465	6	40 <sup>3</sup>	48000	3000	1272, 1272, 1296*
						10	0.581	4	50 <sup>3</sup>		3000	2352, 2544, 2568
						14	0.814	6	56 <sup>3</sup>		6000	6384, 6216, 6480
						18	1.046	4	54 <sup>3</sup>		12000	8664, 8304, 8472
$L_B^B$	10.0	8.6602(8)	0.05812(1)	9 – 27	B	6	0.349	4	48 <sup>3</sup>	48000	1500	2000, 2000**
						8	0.465	6	48 <sup>3</sup>		3000	2000, 6000
						10	0.581	4	50 <sup>3</sup>		6000	2000, 7960
						14	0.814	6	56 <sup>3</sup>		12000	2000, 2000
$L^C$	12.5	10.916(3)	0.04580(1)	11 – 29	A&B	8	0.366	6	48 <sup>3</sup>	36000	2000	1000
						10	0.458	4	50 <sup>3</sup>		3000	4000
						14	0.641	6	56 <sup>3</sup>		6000	7080
						18	0.824	4	72 <sup>3</sup>		12000	2080

TABLE II: Run parameters of the simulations. The number of measurements marked with \* corresponds to the  $R$  values 9 – 15, 17 – 21, 23 – 27 and the ones marked with \*\* to 9 – 15, 17 – 27 respectively.

In figure 4 the results for the total energies are shown against  $R/r_0$ , together with the predictions of the NG spectrum. The energies are rescaled such that  $E_n^{LO} = n$ . The results for the groundstate are completely in agreement with the NG predictions. In this case only the curve of the full spectrum is shown since deviations at different orders of the expansion are not visible on this scale.

For the excited states we were only able to obtain corrected results over a limited range of  $R$ , except for  $E_1$  at  $\beta = 7.5$  where we have results over the full range. For the other  $\beta$  values, the results shown in the plots are the naïve values obtained from Wilson loops with the two largest temporal extents for which we have a reliable signal. In the region where we were able to obtain corrected results we plot them in addition to get an idea of the systematic corrections due to the finite temporal extents of the loops.

We see that the corrected values for  $\beta = 7.5$  follow essentially the Nambu curves, while the results for  $\beta > 7.5$  seem to be pushed away towards the LO lines. However it is to be noted that while for  $\beta = 7.5$  we were able to calculate loops with physical temporal extents between 0.477 and 1.431 fm, we had to progressively reduce  $T$  to between  $\approx 0.35$  fm to 0.824 fm for  $\beta = 10.0$  and 12.5. We believe that this shift is due to contaminations from higher energy states because of the smaller temporal extents of the loops and not because of the different  $\beta$  values. This belief is further reinforced by the fact that in the region where we are able to obtain corrected energies for all values of  $\beta$ , we see good agreement between these values. Also the energies obtained from Wilson loops with equal physical temporal extents agree for the different values of  $\beta$ . This is especially visible for  $E_2$  at  $\beta = 10.0$  and 12.5. A similar effect has earlier been seen in [13]. At smaller values of  $R$  where the difference be-

tween the NG, LO and NLO curves are visible, the data seems to favor the NG curve.

## B. Energy differences

We now turn to the energy differences which are more sensitive to subleading properties of the flux tube. In addition they have the advantage that the constant  $V_0$  does not contribute. The results for the energy differences  $\Delta E_{10}$  and  $\Delta E_{20}$  are shown in figure 5.

Unfortunately we were able to obtain corrected values using eq.(5) only for  $\Delta E_{10}$  at  $\beta = 7.5$ . That data set seems to follow the NG curves quite nicely. For  $\Delta E_{20}$ , our best estimates are the naïve values from eq.(5) with  $T_a = 14$  and  $T_b = 18$ . The physical temporal extents are thus  $> 1$  fm and we expect very little systematic effects in these results. Again we see that the NG curve is favoured by the data.

For  $\Delta E_{10}$  at  $\beta = 10.0$  and 12.5, our best estimates come from the difference  $E_1 - E_0$  with the errors being calculated in quadrature. Even though this gives larger error bars, especially at  $\beta = 12.5$ , we see that both data sets are consistent with  $\beta = 7.5$  values.

For  $\Delta E_{20}$  at  $\beta = 10.0$  and 12.5, the physical temporal extents of the loops are not large enough that the higher order corrections, unaccounted for in equations (4) and (5), are negligible. Nevertheless, for  $\beta = 10.0$ , where it was possible at least partly to take into account the corrections, we see the trend of the data is to follow the NG curve. For  $\beta = 12.5$ , where even that was not possible, the data seems to rise in a straight line and diverge from the string behaviour even at large  $R$ . We however believe that this is due to contamination from the higher states and the corrected data would show the same trend as  $\beta = 7.5$ .

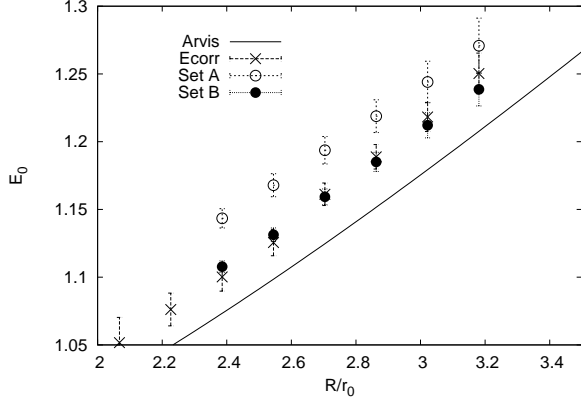


FIG. 3: Comparison of the naïve energy  $\bar{E}_2$  from set A and B.

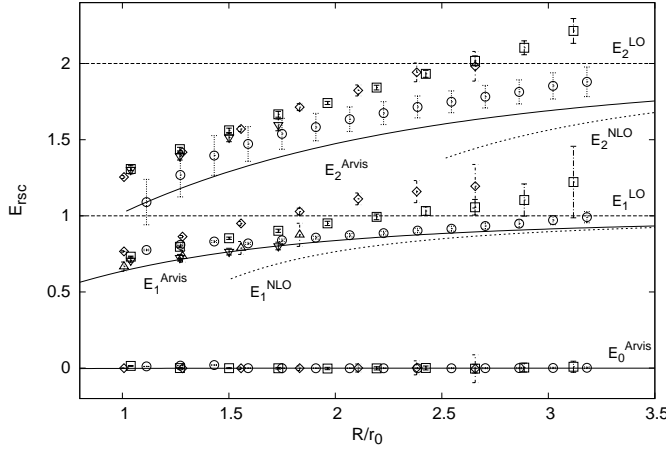


FIG. 4: Results for the total energies  $E_n$ . The  $\circ$ 's are the values for  $\beta = 7.5$ ,  $\square$ 's for  $\beta = 10.0$  and  $\diamond$ 's for  $\beta = 12.5$ .  $\nabla$  are additional corrected values for  $\beta = 10.0$  and  $\triangle$  for  $\beta = 12.5$ . The results have been rescaled, such that  $E_n^{LO} = n$ . The labeling of the lines are as defined in the text.

#### IV. CONCLUSIONS

In this article we have looked at a variant of the multi-level error reduction scheme suitable for studying the excited states of the QCD flux tube. Using this scheme we have looked at the excited states of the flux tube at three different couplings for  $q\bar{q}$  separations between 0.5 to 1.7 fm.

Our results seem to indicate that in this scheme, upto the values of  $R$  we have considered, one needs temporal extents of about 1 fm to make sure that the corrections due to the higher states are well under control. Wherever this criterion has been met, we have seen that the data follows the NG curve.

The corrected data sets for different  $\beta$  values seem to fall on top of each other indicating that there is very little effect due to finite lattice spacing. As such it seems to be much more important to go to larger temporal extents

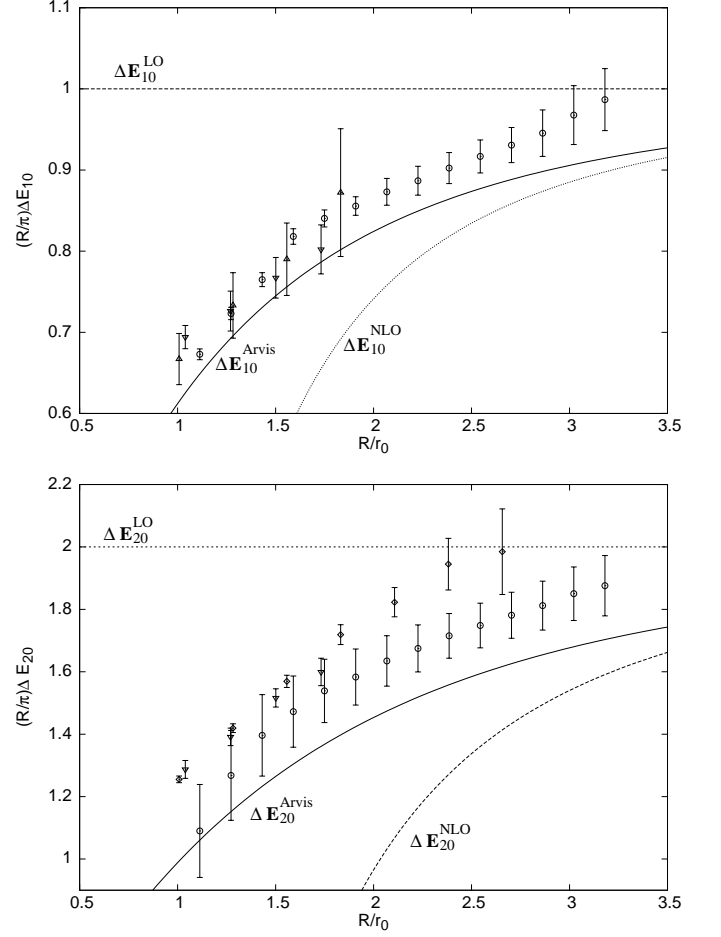


FIG. 5: **Top:** Results for the energy difference  $\Delta E_{10}$ . **Bottom:** Results for the difference  $\Delta E_{20}$ . The mapping of the curves and the points is the same as in the plot for the total energies.

than finer lattices.

Unfortunately our data is still not good enough to distinguish between NG, LW and PS type string theories as that would require a sensitivity at the level of  $R^{-5}$ . Deviations from the NG predictions at higher orders have recently been reported in [21] for gauge duals of random percolation problems.

This was our first attempt to show how to combine the two powerful techniques of multi-level error reduction and sophisticated sources for Wilson loops. Using this we have been able to go to much larger values of  $R$  and  $T$  than was possible before. For ruling out different string models, the error bars will have to be reduced by at least an order of magnitude. That at the moment looks like a project for the future.

#### Acknowledgments

The simulations were distributed over three different computational facilities, namely the computing resources

of the Westfälische Wilhelms-Universität Münster (organized with the condor system [22]), where this study was started, the teraflop Linux cluster KABRU at IMSc, Chennai and the linux cluster LC2 at the ZDV of the Jo-

hannes Gutenberg-Universität Mainz. We are indebted to the institutes for these facilities. BB is funded by the DFG via the SFB 443.

- 
- [1] G. S. Bali, Phys. Rep. **343**, 1 (2001).
  - [2] P. Goddard *et. al.*, Nucl. Phys. **B 56**, 109 (1973).
  - [3] O. Alvarez, Phys. Rev. **D24**, 440 (1981).
  - [4] J.F. Arvis, Phys. Lett. **127B**, 106 (1983).
  - [5] J. Polchinski and A. Strominger, Phys. Rev. Lett. **67**, 1681 (1991).
  - [6] J.M. Drummond, hep-th/0411017; hep-th/0608109.
  - [7] N.D. Hari Dass and P. Matlock, hep-th/0606265; hep-th/0611215; hep-th/0612291.
  - [8] F. Maresca, Ph.D Thesis, Trinity College, Dublin, 2004; J. Kuti, (unpublished).
  - [9] A. Athenodorou, B. Bringoltz and M. Teper, Phys. Lett. **B656**, 132 (2007) arXiv:0709.0693.
  - [10] M. Lüscher, P. Weisz, JHEP **0207**, 049 (2004).
  - [11] J. Kuti, in *Proceedings of the XXIIIrd International Symposium on Lattice field theory*, PoS(Lattice2005), 001 (2005).
  - [12] B.B. Brandt, Diploma thesis, Westfälische Wilhelms-Universität Münster, 2008.
  - [13] P. Majumdar, Nucl. Phys. **B664**, 213 (2003) hep-lat/0211038; hep-lat/0406037 (2004)
  - [14] J. Juge, J. Kuti and C. Morningstar, Phys. Rev. Lett. **90**, 161601 (2003); in Proceedings of Wako 2003, Color confinement and hadrons in quantum chromodynamics, 221, hep-lat/0312019; in Proceedings of Wako 2003, Color confinement and hadrons in quantum chromodynamics, 233, hep-lat/0401032.
  - [15] M. Lüscher and P. Weisz, JHEP **0109**, 010 (2001).
  - [16] M. Lüscher and P. Weisz, JHEP **0407**, 014 (2004).
  - [17] N. D. Hari Dass and P. Majumdar, Phys. Lett. **B658**, 273 (2007) hep-lat/0702019; JHEP **0610**, 020 (2006) hep-lat/0608024
  - [18] B.B. Brandt and P. Majumdar, in *Proceedings of the XXVth International Symposium on Lattice field theory*, PoS(Lattice2007), 027 (2007) arXiv:0709.3379.
  - [19] A. Kennedy and B. Pendleton, Phys. Lett. **156B**, 393 (1985)
  - [20] R. Sommer, Nucl. Phys. **B411**, 839 (1994) hep-lat/9310022
  - [21] P. Giudice, F. Gliozzi and S. Lottini, JHEP **0903**, 104 (2009) arXiv:0901.0748.
  - [22] <http://www.condorproject.org/>, ©1990-2009 Condor team, CSD university of Wisconsin, Madison, WI.
  - [23] At the order where we are comparing the data with the theory, the degeneracies are the same as in the free theory [16]

$\beta$	7.5 set A [17]	10.0 set A 10.0 set B [17]	12.5 set A 12.5 set B [17]
$\sigma$	0.03867(7) 0.038566(6)	0.0206(2) 0.0210(4) 0.020606(4)	0.0128(4) 0.0129(4) 0.012742(17)
$V_0$	0.1730(5)	0.145(3) 0.139(6)	0.124(4) 0.124(4)

TABLE III: Results for the string tension  $\sigma$  and the regularization constant  $V_0$ . The values [17] are the reference results for the string tension.

$R$	$E_0$		$E_1$		$E_2$		$\Delta E_{10}$		$\Delta E_{20}$
$\beta = 7.5$	$T(18, 14)$	$4T$	$T(18, 14)$	$4T$	$T(18, 14)$		$T(18, 14)$	$4T$	$T(18, 14)$
7	0.4251(1)	0.42992(8)	0.753(1)	0.773(2)	0.91(7)		0.328(1)	0.302(3)	0.49(7)
8	0.4660(1)	0.47226(9)	0.768(1)	0.784(2)	0.96(6)		0.302(1)	0.284(2)	0.50(6)
9	0.5064(2)	0.5135(1)	0.785(1)	0.797(3)	0.99(5)		0.279(1)	0.267(3)	0.49(5)
10	0.5464(2)	0.5464(2)	0.806(1)	0.804(2)	1.01(4)		0.259(1)	0.257(3)	0.46(4)
11	0.5863(2)	0.5862(3)	0.828(1)	0.826(2)	1.03(3)		0.242(1)	0.240(3)	0.43(7)
12	0.6259(3)	0.6259(3)	0.853(1)	0.850(2)	1.04(2)		0.227(1)	0.224(3)	0.41(2)
13	0.6655(3)	0.6654(4)	0.879(1)	0.876(3)	1.06(2)		0.214(1)	0.211(3)	0.40(2)
14	0.7049(3)	0.7047(5)	0.907(1)	0.904(3)	1.08(2)		0.202(1)	0.199(3)	0.38(2)
15	0.7442(4)	0.7441(5)	0.936(1)	0.933(3)	1.10(2)		0.192(1)	0.189(3)	0.36(2)
16	0.7835(4)	0.7833(6)	0.966(2)	0.963(3)	1.13(1)		0.183(2)	0.180(4)	0.34(1)
17	0.8228(5)	0.8225(7)	0.998(2)	0.995(4)	1.15(1)		0.175(2)	0.172(4)	0.33(1)
18	0.8620(5)	0.8617(7)	1.030(2)	1.027(4)	1.18(1)		0.168(2)	0.165(4)	0.32(1)
19	0.9012(5)	0.9009(8)	1.064(3)	1.061(5)	1.21(1)		0.162(3)	0.160(5)	0.31(1)
20	0.9404(6)	0.9401(8)	1.097(4)	1.095(6)	1.24(2)		0.157(4)	0.155(6)	0.29(2)
$\beta = 10.0$	$T(18, 14)$	$4T$	$T(18, 14)$	$3T$	$T(10, 8)$		$T(18, 14)$	$4T$	$E_2^B - E_0^A$
9	0.3160(1)	0.3207(1)	0.571(1)	0.563(4)	0.772(4)	0.770(9)	0.255(1)	0.238(3)	0.449(9)
11	0.3599(1)	0.3596(5)	0.587(1)	0.567(6)	0.770(3)	0.757(7)	0.227(2)	0.225(3)	0.397(7)
13	0.4032(2)	0.4026(8)	0.609(2)	0.588(5)	0.780(3)	0.769(7)	0.206(2)	0.204(3)	0.366(7)
15	0.4460(2)	0.445(1)	0.634(2)	0.613(5)	0.794(4)	0.780(8)	0.188(2)	0.186(4)	0.335(8)
17	0.4884(3)	0.487(1)	0.663(3)		0.809(2)		0.175(3)	0.174(3)	0.322(2)
19	0.5309(3)	0.529(2)	0.694(3)		0.834(3)		0.163(3)	0.162(4)	0.305(3)
21	0.5733(4)	0.571(2)	0.726(4)		0.860(3)		0.152(4)	0.152(5)	0.289(4)
23	0.6153(5)	0.613(4)	0.757(7)		0.889(4)		0.142(7)	0.140(10)	0.276(6)
25	0.6575(8)	0.655(4)	0.79(1)		0.919(6)		0.14(1)	0.135(15)	0.264(7)
27	0.699(2)	0.697(4)	0.84(3)		0.954(10)		0.14(3)	0.136(14)	0.257(11)
$\beta = 12.5$	$T(18, 14)$	$4T$	$T(18, 10)$	$3T$	$T(14, 10)$		$T(18, 10)$	$3T$	$E_2^B - E_0^A$
11	0.2540(2)	0.2535(5)	0.472(1)	0.444(9)	0.612(3)		0.218(1)	0.192(10)	0.358(3)
14	0.2953(3)	0.2945(9)	0.488(2)	0.459(9)	0.613(3)		0.192(2)	0.167(10)	0.318(3)
17	0.3359(4)	0.335(1)	0.510(2)	0.481(8)	0.625(3)		0.173(2)	0.149(10)	0.290(3)
20	0.3761(6)	0.374(2)	0.536(3)	0.512(12)	0.644(4)		0.158(3)	0.141(9)	0.269(4)
23	0.4162(9)	0.414(4)	0.566(5)		0.663(5)		0.147(5)		0.249(6)
26	0.456(1)	0.453(6)	0.593(9)		0.688(7)		0.134(9)		0.234(9)
29	0.496(2)	0.492(10)	0.622(16)		0.707(11)		0.122(16)		0.215(15)

TABLE IV: Results of the simulations. The left column corresponds to the naive value of loops, obtained from Wilson loops with the temporal extents given in brackets in the header. The right column corresponds to the corrected value of a fit to the form (4),(5), wherever this was possible. The header  $4T$  means, that the values below were obtained from fits to the values from all combinations of the four different temporal extents, and the header  $3T$  means that only the three lowest temporal extents were used for the fits.